Highlights

The Beggining of Control Revolution: Ofset-free Koopman MPC

Patrik Valábek

- Research highlight 1

- Research highlight 2

The Beggining of Control Revolution: Ofset-free Koopman MPC

Patrik Valábek

ªSTU, Redlinskeho 9, Bratislava, Slovakia

Abstract

Keywords:

1. Introduction

2. Preliminaries and Notation

2.1. Offset-Free MPC

2.2. Nonlinear MPC

2.3. Koopman Operator for Control

2.4. Koopman MPC

2.5. State Estimation - Observer

3. Koopman MPC with Offset-Free - Baseline

In this section, we will present a standard offset free optimal framework consisting of Target Optimization, State Estimation - Observer and MPC. As observer is standard Kalman filter or extended Kalman filter, we will discuss mainly remaining two optimization problems. Both remaining components had to be designed in a way that they are able to work with the Koopman operator. The main goal of this section is to show that the standard formulation can be easily transformed for the offset-free MPC use.
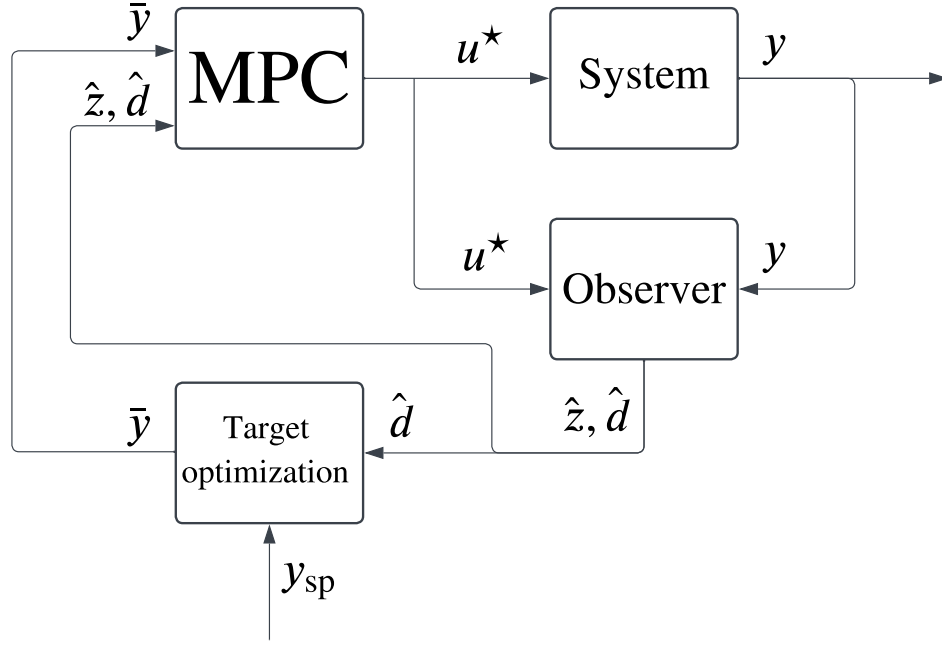
Figure 1: Closed-loop control structure.

3.1. Target Optimization

$$\min_{\bar{u},\bar{z},\bar{y}} \quad (\bar{y} - y_{\text{ref}})^{\mathsf{T}} Q_{\text{y}}(\bar{y} - y_{\text{ref}}) \tag{1a}$$

$$\text{s.t.} \quad \bar{z} = A\bar{z} + B\bar{u} \tag{1b}$$

$$\bar{y} = C\bar{z} + d \tag{1c}$$

$$u_{\min} \le \bar{u} \le u_{\max} \tag{1d}$$

$$y_{\min} \le \bar{y} \le y_{\max} \tag{1e}$$

$$d = \hat{d}(t), \quad y_{\text{ref}} = y_{\text{sp}} \tag{1f}$$

2

3.2. MPC

$$\min_{u_0,\ldots,u_{N-1}} \sum_{k=0}^{N-1}(y_k - \bar{y})^\intercal Q_{\mathrm{y}}(y_k - \bar{y}) + \sum_{k=0}^{N-1}\Delta u_k^\intercal Q_{\mathrm{u}}\Delta u_k, \tag{2a}$$

$$\text{s.t.}\quad z_{k+1} = Az_k + Bu_k, \quad k \in \mathbb{N}_0^{N-1}, \tag{2b}$$

$$y_k = Cz_k + d, \quad k \in \mathbb{N}_0^{N-1}, \tag{2c}$$

$$\Delta u_k = u_k - u_{k-1}, \quad k \in \mathbb{N}_0^{N-1}, \tag{2d}$$

$$u_{\min} \le u_k \le u_{\max}, \quad k \in \mathbb{N}_0^{N-1}, \tag{2e}$$

$$y_{\min} \le y_k \le y_{\max}, \quad k \in \mathbb{N}_0^{N-1}, \tag{2f}$$

$$z_0 = \hat{z}(t), \quad d = \hat{d}(t), \quad u_{-1} = u(t - T_{\mathrm{s}}) \tag{2g}$$

3.3. Closed-Loop Control Structure

4. Koopman MPC with Offset-Free - Proposed

Main drawback that we observe in a current Koopman MPC (offset-free, robust, or any other), is that the optimization is done without leveraging knowledge of the lifted space. Of course we are predicting in the lifted space, but in objective function we are using original space, that is created derived as linear transformation of the lifted space $y_k = Cz_k$. This transformation is not linear by nature $y_k = h(z_k)$, but to use linear MPC, we think we had no other choice. Some papers are not using this transformation directly, but after closer look, they are usually using equivalent transformations, for example expanding lifted space with measurements, but dynamic in lifted space is linear, so transformations to achieve back this measurements is linear. We will show that we can use the lifted space directly in the objective function, showing how to handle the lifted space and transformation of an objective function. We can fully eliminate the neccessity of the back transformation used in objective function in MPC, but we still need them to compute the target for the lifted space. In this case and case of constraints, we use a first order Taylor expansion, to better approximate the transformation.

4.1. Target Optimization

The objective function of target estimation is the same as in the standard offset-free MPC. The main difference is in

The proposed target optimization problem is formulated as:

$$\min_{\bar{u},\bar{z},\bar{y}} \quad (\bar{y} - y_{\text{ref}})^{\mathsf{T}} Q_{\text{y}} (\bar{y} - y_{\text{ref}}), \tag{3a}$$

$$\text{s.t.} \quad \bar{z} = A\bar{z} + B\bar{u}, \tag{3b}$$

$$\bar{y} = H(z_{\text{LP}})\bar{z} + h(z_{\text{LP}}) - H(z_{\text{LP}})z_{\text{LP}} + d, \tag{3c}$$

$$u_{\min} \leq \bar{u} \leq u_{\max}, \tag{3d}$$

$$y_{\min} \leq \bar{y} \leq y_{\max}, \tag{3e}$$

$$d = \hat{d}(t), \quad y_{\text{ref}} = y_{\text{sp}}, \quad z_{\text{LP}} = \bar{z}_{-1}, \tag{3f}$$

where $H(z_{\text{LP}})$ is the Jacobian of the transformation $h(z_{\text{LP}})$. z_{LP} is a linearization point, the point where we approximate our function with first order Taylor expansion. We propose, that this point should be as close as possible to the $\bar{z}$. Therefor we are using the previously calculated target $\bar{z}_{-1}$. This allow us to better approximate the transformation of the lifted space to the original space and more precise target optimization.

4.2. MPC

The proposed MPC problem is formulated as:

$$\min_{u_0,\dots,u_{N-1}} \quad \sum_{k=0}^{N-1} (z_k - \bar{z})^{\mathsf{T}} Q_{\text{z}} (z_k - \bar{z}) + \sum_{k=0}^{N-1} \Delta u_k^{\mathsf{T}} Q_{\text{u}} \Delta u_k, \tag{4a}$$

$$\text{s.t.} \quad z_{k+1} = Az_k + Bu_k, \quad k \in \mathbb{N}_0^{N-1}, \tag{4b}$$

$$y_k = H(z_0)z_k + h(z_0) - H(z_0)z_0 + d, \quad k \in \mathbb{N}_0^{N-1}, \tag{4c}$$

$$\Delta u_k = u_k - u_{k-1}, \quad k \in \mathbb{N}_0^{N-1}, \tag{4d}$$

$$u_{\min} \leq u_k \leq u_{\max}, \quad k \in \mathbb{N}_0^{N-1}, \tag{4e}$$

$$y_{\min} \leq y_k \leq y_{\max}, \quad k \in \mathbb{N}_0^{N-1}, \tag{4f}$$

$$z_0 = \hat{z}(t), \quad d = \hat{d}(t), \quad u_{-1} = u(t - T_{\text{s}}) \tag{4g}$$

where $H(z_0)$ is the Jacobian of the transformation $h(z_0)$ at the point z_0. This linearization point is chosen to best approximate the surroundings of current operational point. The first order Taylor expansion is done to receive y_k, which is used only in the constrains of the system. In objective funtion, we use a tuning matric Q_{z} to penalize the difference from lifted space target. We propose to derive this tuning matrix as follows:

$$Q_{\text{z}} = H(\bar{z})^{\mathsf{T}} Q_{\text{y}} H(\bar{z}). \tag{5}$$

4

This allows us to use and tune our problem using matrix Q_y, which is convenient and easily tuned. This is a significant change from the standard Koopman MPC, where the objective function is defined in the original space.

4.3. Closed-Loop Control Structure

5. Block Diagonal Deep Koopman Transformation

TODO: split this section into theory and simulation evaluation, bevare notation conflict zbar   During our work, we encounter a several problems with the suboptimal or infeasible solutions using Koopman MPC using Gurobi solver. For the enhancement of the performaance, we are proposing a block diagonal structure of the matrix A. This transformation can be done after obtaining the Koopman operator, with finding the transformation matrix T that transforms the Koopman operator to the block diagonal form:

$$\bar{A} = T^{-1}AT. \tag{6}$$

This transformation is done by finding the eigenvalues and eigenvectors of the Koopman operator, and then grouping them into blocks. The transformation matrix T is constructed from the eigenvectors, and the block diagonal form $\bar{A}$ is obtained by applying the transformation to the original Koopman operator A. Using this approach, we had to modify the rest of the model accordingly, using the transformation matrix T to transform the input and output matrices B and C as well as the lifted states z:

$$\bar{B} = T^{-1}B, \quad \bar{C} = CT, \quad \bar{z}_k = T^{-1}z_k. \tag{7}$$

When computing the Jackobian, we are transforming the original Jackobian $H(z_k)$ to the block diagonal form $\bar{H}(z_k)$ using the transformation matrix T:

$$\bar{H}(z_k) = H(z_k)T = H(T\bar{z}_k)T. \tag{8}$$

After this transformation we are able to enhace the performance in optimization as can be seen in Table 1. This table is done using the formulation of Koopman MPC which can be seen in Sec. 3. The table shows the decrease in a computational times. Also with this formulation we are able to obtain optimal solution 100% time during simulation. Contrary, the full Koopman MPC formulation is able to obtain optimal solution only 26.7% of the time with the rest of the time giving warning, that the solution is suboptimal.

Table 1: Comparison of structure of problem to solver time and control performance.

Structure	Time TE/MPC	Optimal? [%]	OBJ	ST h_1	ST h_2
Full	0.2392 / 2.3884	26.7	100.0	43	48
Block Diagonal	0.2191 / 1.6204	100.0	94.1	25	31

We can see also increase in a control performance, which is measured by the objective function value, which is in optimal case arounf 6% lower. Also the settling time for both levels is lower.

The second option how to obtain the block diagonal structure is to learn the Koopman operator directly in the block diagonal form. This can be done by limiting the number of learnable parameters in a Koopman matrix during training to those that are in the block diagonal form. This also speeds the training as less parameters are learned.

To obtain an optimal performance, which is neccessary for the real time control, we are proposing to use the block diagonal structure of the Koopman operator. There is no neccessity to use the full Koopman operator, as the block diagonal structure is able to capture the same dynamics of the system and favors the optimization performance. The way this structure is obtained, during or after the training, is not important, as long as the Koopman operator is in the block diagonal form.

6. Simulation Setup

7. Simulation Results

In the following, we make precise the output mappings sketched in the notes and list the combinations (setups) evaluated in the simulations.

7.1. Output mappings for target and prediction

We consider three alternatives for computing the steady-state output corresponding to a candidate steady-state lifted state $\bar{z}_k$ and disturbance estimate $\hat{d}_k$:

$$\text{T1:} \quad \bar{y}_k = C\,\bar{z}_k + \hat{d}_k, \tag{9a}$$

$$\text{T2:} \quad \bar{y}_k = h(\bar{z}_{k-1}) + J_{\bar{z}_{k-1}}\left(\bar{z}_k - \bar{z}_{k-1}\right) + \hat{d}_k, \tag{9b}$$

$$\text{T3:} \quad \bar{y}_k = h(\hat{z}_k) + J_{\hat{z}_k}\left(\bar{z}_k - \hat{z}_k\right) + \hat{d}_k. \tag{9c}$$

Here, $h(\cdot)$ denotes the measurement/lifted-to-output map, and J_z its Jacobian evaluated at z.

For dynamic prediction over the horizon, with disturbance held at the current estimate $\hat{d}_k$, we use four alternatives for the output of a predicted lifted state z_{k+i}:

$$\text{D1:}\quad y_{k+i} = C\,z_{k+i} + \hat{d}_k, \tag{10a}$$

$$\text{D2:}\quad y_{k+i} = h(\bar{z}_{k-1}) + J_{\bar{z}_{k-1}}\left(\bar{z}_{k+i} - \bar{z}_{k-1}\right) + \hat{d}_k, \tag{10b}$$

$$\text{D3:}\quad y_{k+i} = h(\hat{z}_k) + J_{\hat{z}_k}\left(\bar{z}_{k+i} - \hat{z}_k\right) + \hat{d}_k, \tag{10c}$$

$$\text{D4:}\quad y_{k+i} = h(\bar{z}_k) + J_{\bar{z}_k}\left(z_{k+i} - \bar{z}_k\right) + \hat{d}_k. \tag{10d}$$

7.2. Simulation Results for Two Tanks System

We index target mappings by T1–T3 and dynamic mappings by D1–D4 as in (9)–(10). The simulation setups below pair one target mapping with one dynamic mapping:

Table 2: Simulation setups matrix, with Qy much higher Qu; Qy = diag(5) Qu = diag(0.1). Columns: dynamic mappings (D1–D4). Rows: target mappings (T1–T3). Fill cells with the identifier/value for each tested combination. NMPC benchmark is 100.

		DM		
TM	D1	D2	D3	D4
T1	124.19	x	x	x
T2	x	104.86	107.47	103.79
T3	x	105.34	108.11	103.89

Table 3: Simulation setups matrix, with Qy and Qu with equal diagonal values (5). Columns: dynamic mappings (D1–D4). Rows: target mappings (T1–T3). NMPC benchmark is 100.

		DM		
TM	D1	D2	D3	D4
T1	112.90	x	x	x
T2	x	108.86	106.44	107.52
T3	x	106.24	108.94	105.33

Table 4: Simulation setups matrix, with Qy much lower Qu; Qy = diag(0.1) Qu = diag(5). Columns: dynamic mappings (D1–D4). Rows: target mappings (T1–T3). NMPC benchmark is 100.

| | DM | | | |
TM	D1	D2	D3	D4
T1	147.49	x	x	x
T2	x	189.52	176.33	190.96
T3	x	143.29	143.86	143.47

7.3. Simulation Results for Two Reactor System

We index target mappings by T1–T3 and dynamic mappings by D1–D4 as in (9)–(10). The simulation setups below pair one target mapping with one dynamic mapping:

Table 5: Simulation setups matrix, with Qy much higher Qu; Qy = diag(5) Qu = diag(0.1). Columns: dynamic mappings (D1–D4). Rows: target mappings (T1–T3). NMPC benchmark is 100.

| | DM | | | |
TM	D1	D2	D3	D4
T1	365.0	x	x	x
T2	x	251.5	250.7	255.5
T3	x	259.0	265.1	263.2

8. Pasteurization Unit: Experimental Device

The experimental validation of the proposed control strategy is conducted on a laboratory-scale pasteurization unit, a thermal processing system designed for educational and research purposes. This apparatus, depicted in Figure 2, represents a complex multivariable thermal system commonly encountered in food processing industries, where precise temperature regulation is crucial for product quality and safety.

Table 6: Simulation setups matrix, with Qy and Qu with equal diagonal values (1). Columns: dynamic mappings (D1–D4). Rows: target mappings (T1–T3). NMPC benchmark is 100.

TM	DM			
	D1	D2	D3	D4
T1	184.5	x	x	x
T2	x	146.2	146.8	146.2
T3	x	150.6	153.9	150.6

Table 7: Simulation setups matrix, with Qy much lower Qu; Qy = diag(0.1) Qu = diag(5). Columns: dynamic mappings (D1–D4). Rows: target mappings (T1–T3). NMPC benchmark is 100.

TM	DM			
	D1	D2	D3	D4
T1	130.4	x	x	x
T2	x	112.1	112.5	112.2
T3	x	115.5	116.1	115.6

Figure 2: Pasteurization unit experimental apparatus.

8.1. System Configuration

The pasteurization unit comprises a tubular heat exchanger configuration with counter-current flow arrangement, as illustrated schematically in Figure 3. The system consists of two primary fluid circuits: the product circuit and the heating medium circuit. The product fluid is pumped through a helical tube nested within a cylindrical shell, where it exchanges thermal energy with hot water circulating in the shell side.
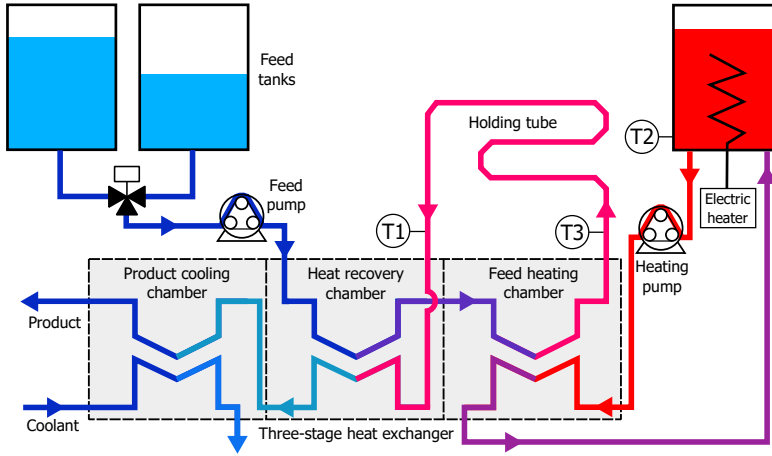
Figure 3: Schematic representation of the heat exchanger configuration.

The unit features eight manipulated variables that can be adjusted for process control:

- `Pump1`: Product feed flow rate control (%)

- `Pump2`: Heating medium circulation rate (%)

- `Heater`: Electric heater power for the heating medium (%)

- `DV`: Diversion valve position

- `FSV`: Feed selection valve

- `CWV`: Cooling water valve position

- `TAFV`, `TBFV`: Tank flow control valves

The system is instrumented with multiple sensors providing real-time measurements, including four temperature sensors (`T1`–`T4`) positioned at strategic locations along the product and heating circuits, a flow meter (`F1`) measuring product flow rate, a level sensor (`L1`) for tank monitoring, and additional auxiliary measurements for comprehensive process monitoring.

8.2. Control Configuration

For the experimental implementation, the control objective focuses on regulating the outlet product temperature (`T4`) to track desired setpoint trajectories. The primary manipulated variable is the heating medium flow rate (`Pump2`), which directly influences the thermal energy transferred to the product stream. Additionally, a cascade control structure is employed for the heater, where the electric heater power is modulated to maintain a constant heating medium inlet temperature (`T2`), providing a stable thermal source. The product feed rate (`Pump1`) acts as a measurable disturbance, creating varying thermal loads that challenge the controller's disturbance rejection capabilities.

The system exhibits typical characteristics of thermal processes, including significant time delays, nonlinear behavior due to temperature-dependent fluid properties, and strong coupling between flow rates and temperatures. These features make it an ideal testbed for evaluating advanced control strategies such as the proposed offset-free Koopman MPC framework.

8.3. Data Acquisition and Control Platform

The experimental apparatus is integrated with a distributed control system accessible through the ELab platform, which provides remote monitoring and control capabilities via a web-based SCADA interface. The control algorithms are implemented in MATLAB/Simulink environment with a sampling period of 1 s, enabling real-time control execution. All process variables are logged continuously for post-experiment analysis and performance evaluation.

9. Experimental Results

10. Discussion

11. Conclusion

Appendix A. System Models

In this appendix, we provide detailed mathematical descriptions of the two benchmark nonlinear systems used to evaluate the proposed offset-free Koopman MPC schemes: a two-tank system with hydraulic flows and a two-reactor CSTR series with recycle and parallel reactions.

Appendix A.1. Two Tanks System

The two-tank system consists of two interconnected tanks with liquid heights h_1 and h_2. Each tank receives an inflow (control inputs u_1 and u_2, respectively), and liquid can flow between tanks and out of the system through gravity-driven mechanisms. The continuous-time nonlinear dynamics are described by:

$$\frac{dh_1}{dt} = \frac{1}{A_1} \left(u_1 - q_{12} \right), \tag{A.1a}$$

$$\frac{dh_2}{dt} = \frac{1}{A_2} \left(u_2 + q_{12} - q_{\text{out}} \right), \tag{A.1b}$$

where A_1 and A_2 are the cross-sectional areas of tanks 1 and 2, respectively. The inter-tank flow q_{12} and the outlet flow q_{out} follow nonlinear hydraulic relationships:

$$q_{12} = k_1 \, \text{sgn}(h_1 - h_2) \sqrt{|h_1 - h_2|}, \tag{A.2}$$

$$q_{\text{out}} = k_2 \sqrt{h_2}, \tag{A.3}$$

with k_1 and k_2 being flow coefficients. The outputs are the measured tank heights:

$$y = \begin{bmatrix} h_1 \\ h_2 \end{bmatrix}. \tag{A.4}$$

The system is discretized with a sampling time $T_s = 1\,\text{s}$ using a Runge–Kutta integration scheme. The physical parameters and operational constraints used in the simulations are summarized in Table A.8.

12

Table A.8: Two-tank system parameters and operational constraints.

Parameter	Description	Value
A_1	Cross-sectional area of tank 1	$1.0\,\mathrm{m}^2$
A_2	Cross-sectional area of tank 2	$1.0\,\mathrm{m}^2$
k_1	Inter-tank flow coefficient	$0.5\,\mathrm{m}^{2.5}/\mathrm{s}$
k_2	Outlet flow coefficient	$0.3\,\mathrm{m}^{2.5}/\mathrm{s}$
$h_1^0,\ h_2^0$	Initial heights	$0.5\,\mathrm{m}$
$u_1^0,\ u_2^0$	Initial inflows	$0.0705, 0.4759\,\mathrm{m}^3/\mathrm{s}$
$u_1 \in$	Inflow constraint (tank 1)	$[0.0, 0.5]\,\mathrm{m}^3/\mathrm{s}$
$u_2 \in$	Inflow constraint (tank 2)	$[0.0, 1.0]\,\mathrm{m}^3/\mathrm{s}$
T_s	Sampling time	$1.0\,\mathrm{s}$

Appendix A.2. Two Reactor System

The two-reactor system consists of two continuous stirred tank reactors (CSTRs) in series with a recycle loop from the second reactor back to the first. Each reactor is equipped with jacket cooling. The system models a classic selectivity problem with parallel competing reactions on reactant A.

Appendix A.2.1. Chemical Reactions

Three reaction pathways are considered:

$$\text{(R1) Desired:} \quad 2\,\mathrm{A} \to \mathrm{B}, \qquad r_1 = k_1(T)\,C_A^2, \qquad \text{(A.5)}$$
$$\text{(R2) Undesired:} \quad \mathrm{A} \to \mathrm{U}, \qquad r_2 = k_2(T)\,C_A, \qquad \text{(A.6)}$$
$$\text{(R3) Shunt (R1 only):} \quad \mathrm{A} + \mathrm{B} \to 2\,\mathrm{B}, \qquad r_3 = k_3(T)\,C_A\,C_B, \qquad \text{(A.7)}$$

where the temperature-dependent rate constants follow Arrhenius kinetics:

$$k_i(T) = k_{i,0}\,\exp\left(-\frac{E_i}{RT}\right), \quad i = 1, 2, 3. \qquad \text{(A.8)}$$

The autocatalytic shunt reaction (R3) occurs only in the first reactor.

Appendix A.2.2. Dynamic Model

The system has eight states:

$$x = \begin{bmatrix} C_{A,1} & T_1 & C_{A,2} & T_2 & C_{B,1} & C_{B,2} & C_{U,1} & C_{U,2} \end{bmatrix}^\top, \qquad \text{(A.9)}$$

13

where $C_{A,i}$, $C_{B,i}$, and $C_{U,i}$ denote concentrations of species A, B, and U in reactor i, and T_i is the temperature. The four control inputs are:

$$u = \begin{bmatrix} F & L & T_{c,1} & T_{c,2} \end{bmatrix}^\top, \tag{A.10}$$

with F the fresh feed flow rate, L the recycle flow rate, and $T_{c,i}$ the jacket coolant temperatures.

The continuous-time dynamics are:

$$\frac{dC_{A,1}}{dt} = \frac{1}{V_1}\big[C_{A,0}\,F + L\,C_{A,2} - (F+L)\,C_{A,1}\big] - 2\,r_{1,1} - r_{2,1} - r_{3,1}, \tag{A.11a}$$

$$\frac{dC_{B,1}}{dt} = \frac{1}{V_1}\big[C_{B,0}\,F + L\,C_{B,2} - (F+L)\,C_{B,1}\big] + r_{1,1} + r_{3,1}, \tag{A.11b}$$

$$\frac{dC_{U,1}}{dt} = \frac{1}{V_1}\big[C_{U,0}\,F + L\,C_{U,2} - (F+L)\,C_{U,1}\big] + r_{2,1}, \tag{A.11c}$$

$$\frac{dT_1}{dt} = \frac{1}{V_1}\big[T_0\,F + L\,T_2 - (F+L)\,T_1\big] - \frac{U_1 A_1}{V_1\,\rho\,c_p}(T_1 - T_{c,1})$$
$$\qquad + \frac{1}{\rho\,c_p}\big[(-\Delta H_1)\,r_{1,1} + (-\Delta H_2)\,r_{2,1} + (-\Delta H_3)\,r_{3,1}\big], \tag{A.11d}$$

$$\frac{dC_{A,2}}{dt} = \frac{F+L}{V_2}\big[C_{A,1} - C_{A,2}\big] - 2\,r_{1,2} - r_{2,2}, \tag{A.11e}$$

$$\frac{dC_{B,2}}{dt} = \frac{F+L}{V_2}\big[C_{B,1} - C_{B,2}\big] + r_{1,2}, \tag{A.11f}$$

$$\frac{dC_{U,2}}{dt} = \frac{F+L}{V_2}\big[C_{U,1} - C_{U,2}\big] + r_{2,2}, \tag{A.11g}$$

$$\frac{dT_2}{dt} = \frac{F+L}{V_2}\big[T_1 - T_2\big] - \frac{U_2 A_2}{V_2\,\rho\,c_p}(T_2 - T_{c,2})$$
$$\qquad + \frac{1}{\rho\,c_p}\big[(-\Delta H_1)\,r_{1,2} + (-\Delta H_2)\,r_{2,2}\big], \tag{A.11h}$$

where $r_{j,i}$ denotes the rate of reaction j in reactor i. The outputs are all eight states:

$$y = x. \tag{A.12}$$

The system is discretized with sampling time $T_s = 1\,\text{s}$ using a Runge–Kutta integration scheme. Physical parameters, kinetic constants, and operational constraints are listed in Tables A.9–A.11.

Table A.9: CSTR series physical and thermodynamic parameters.

Parameter	Description	Value
V_1	Volume of reactor 1	$1.0 \times 10^{-3}\,\text{m}^3$
V_2	Volume of reactor 2	$2.0 \times 10^{-3}\,\text{m}^3$
$U_1 A_1$	Heat transfer coefficient $\times$ area (R1)	$0.461\,\text{kJ/(s·K)}$
$U_2 A_2$	Heat transfer coefficient $\times$ area (R2)	$0.732\,\text{kJ/(s·K)}$
ρ	Liquid density	$1050\,\text{kg/m}^3$
c_p	Specific heat capacity	$3.766\,\text{kJ/(kg·K)}$
R	Universal gas constant	$8.3145 \times 10^{-3}\,\text{kJ/(mol·K)}$
$C_{A,0}$	Feed concentration of A	$97.35\,\text{mol/m}^3$
$C_{B,0}, C_{U,0}$	Feed concentrations of B, U	$0.0\,\text{mol/m}^3$
T_0	Feed temperature	$298.0\,\text{K}$

Table A.10: Arrhenius kinetic parameters for reactions R1–R3.

Reaction	Parameter	Pre-exponential	Activation Energy	Heat of Reac
R1: $2\,\text{A} \rightarrow \text{B}$	$k_{1,0}, E_1, \Delta H_1$	$1.0 \times 10^5\,\text{m}^3/(\text{mol·s})$	$45.0\,\text{kJ/mol}$	$60.0\,\text{kJ/mol}$
R2: $\text{A} \rightarrow \text{U}$	$k_{2,0}, E_2, \Delta H_2$	$9.8 \times 10^9\,\text{s}^{-1}$	$70.0\,\text{kJ/mol}$	$40.0\,\text{kJ/mol}$
R3: $\text{A} + \text{B} \rightarrow 2\,\text{B}$	$k_{3,0}, E_3, \Delta H_3$	$5.0 \times 10^4\,\text{m}^3/(\text{mol·s})$	$55.0\,\text{kJ/mol}$	$60.0\,\text{kJ/mol}$

Table A.11: CSTR series operational constraints and initial conditions.

Parameter	Description	Value/Range
$F \in$	Fresh feed flow rate	$[0.0, 2.0 \times 10^{-4}]\,\text{m}^3/\text{s}$
$L \in$	Recycle flow rate	$[0.0, 2.0 \times 10^{-4}]\,\text{m}^3/\text{s}$
$T_{c,1}, T_{c,2} \in$	Coolant temperatures	$[280.0, 330.0]\,\text{K}$
x_0	Initial state (steady state)	Computed for $u_0 = [1.5 \times 10^{-4}, 7.5 \times 10^{-5}, 290, 290]^\top$
T_s	Sampling time	$1.0\,\text{s}$